

LONG-PERIOD OSCILLATIONS IN A HARBOUR WITH FLUID MUD BOTTOM

Wataru KIOKA¹, M. Akter HOSSAIN² and Kenji KASHIHARA³

ABSTRACT

Non-linear dynamic responses of fluid mud to the oscillating surface waves in a harbour basin and their consequential effects on the long-period harbour excitations are investigated. A set of Boussinesq-type equations based on the weakly nonlinear, dispersive and viscous wave theories is developed for coupled two-layer density stratified system, incorporating the boundary layer corrections for the interfacial shear and mud viscosity. Laboratory experiments are also conducted with fluid mud for different wave periods, and the generation, behavior and different propagation modes of the interfacial waves are examined. Both experimental and numerical results demonstrate that the amplification of water surface displacements is significantly reduced near the first peak of resonance oscillations in the harbour where the internal mode of the interfacial waves governs the surface mode in the motion of the interface. Near the second peak of resonance oscillations the surface mode of the interfacial waves dominates and the interface oscillates nearly in phase of surface waves. The amplification of water surface displacements at the second peak is also reduced to some extent.

1. INTRODUCTION

In many harbours with silty sediment bed, the stratified system of water waves overlying a fluid mud layer or suspended sediment layer frequently occurs. Such dense lower layer may have significant effects on the harbour excitations induced by

¹Professor, ²Graduate Student and ³Research Associate: Department of Civil Engineering, Nagoya Institute of Technology, Gokiso-cho, Showa-ku, Nagoya 466-8555, Japan

long-period waves. Many studies have so far been conducted addressing the long-period excitations in harbours, but all the previous studies were based on the assumption that the bottom of the harbour is rigid and non-responsive to the surface waves. The behavior of soft mud bed in a harbour and its interaction with water surface waves are yet to be understood. In this study, the excitations induced by long-period waves in a harbour with soft mud bed are investigated. Generation of interfacial waves, their behaviors and different propagation modes are examined. Effects of bottom mud on the harbour excitations induced by the long-period waves are also analyzed.

For theoretical formulations, we adopted here a two-layer density stratified fluid system with lower layer as the fluid mud, and a set of Boussinesq-type equations based on the weakly nonlinear, dispersive and viscous wave theories is developed describing the nonlinear interaction of fluid mud with the propagating surface waves. The behavior of mud depends on the wave induced internal stresses, and the soft mud can behave elastically at very low strain, visco-elastically at intermediate strain and viscously at the high strain level (Foda et al., 1993). Since the resonant long-period oscillations may induce relatively high oscillatory strains in the mud, the present model assumes that the mud becomes fluidized and behaves like a viscous fluid (Dalrymple and Liu, 1978). For the verification of numerically predicted results from the adopted model, laboratory experiments are also conducted with fluid mud for different incident wave periods.

Long-period oscillations in a harbour are of concern because such oscillations are often responsible for disturbing the operations of ship terminals, for breaking the mooring of vessels and for flooding on the wharf. Countermeasure against such harbour excitations is however not yet established owing to the difficulty of controlling the incident long waves by means of conventional breakwaters. The present study is also aimed to investigate the behavior of fluidized mud inside the harbour, and thereby addresses the possible means of controlling the harbour excitations using fluidized mud. Since the wave heights inside the harbour are usually too small to liquefy the silty harbour bed, a fluidized sediment bed may be artificially generated by boiling (see Takahashi et al., 1994).

2. THEORETICAL FORMULATION

2.1 Governing Equations

A definition sketch of the two-layer fluid system adopted for the theoretical model is presented in Fig.1. The surface wave is propagating in water depth h over a dense mud layer of thickness d . Beneath the lower denser fluid mud, we assumed a rigid impermeable bed. In the analysis, the density-stratified fluid is confined to a harbour basin. The density and viscosity are respectively denoted by ρ and ν , and the subscripts 1 and 2 stand for upper and lower layers respectively. The governing equations for the fluid motion are the continuity and Navier-Stokes equations for an

incompressible fluid. For the simplicity, the mathematical formulations described hereinafter are only for the two-dimensional motion.

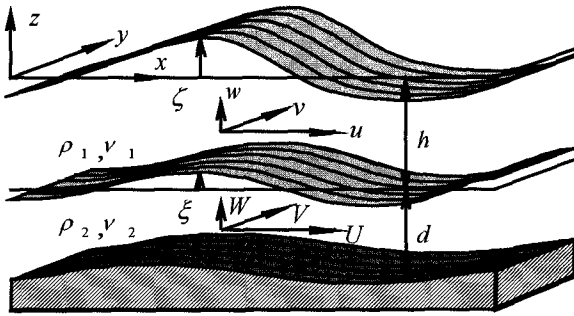


Fig. 1. Definition sketch

The dynamic and kinematic boundary conditions at the free-surface are given by

$$p_1 = 0 \quad (z = \zeta) \quad (1)$$

$$w = \zeta_t + u\zeta_x \quad (z = \zeta) \quad (2)$$

where p_1 is the pressure, u and w are respectively the horizontal and vertical velocities in the upper layer, and ζ is the free-surface displacement. The subscripts x and t indicate the partial derivatives. At the water-mud interface, the following boundary conditions are imposed:

$$p_1 - 2\rho_1\nu_1w_z = p_2 - 2\rho_2\nu_2(W + \hat{W})_z \quad (z = -h + \xi) \quad (3)$$

$$\{u - (U + \hat{U})\}\xi_x - \{w - (W + \hat{W})\} = 0 \quad (z = -h + \xi) \quad (4)$$

$$(U + \hat{U})_z + (W + \hat{W})_x = 0 \quad (z = -h + \xi) \quad (5)$$

$$u = U + \hat{U} \quad (z = -h + \xi) \quad (6)$$

where U and W are the horizontal and vertical velocities in the lower layer respectively, \hat{U} and \hat{W} are the horizontal and vertical rotational velocities at the interface for the lower layer respectively, ξ is the interfacial displacement, and p_2 is the pressure in the lower layer. The subscripts x and z indicate the partial derivatives. Eqs. (3), (4), (5) and (6) are respectively the condition for normal stress continuity, the usual kinematic condition, the condition for shear stress continuity and the continuity of horizontal velocity. The viscous effects of upper fluid are assumed very small, and the rotational velocities at the interface are disregarded in the upper layer. This assumption will be discussed in the following section.

The boundary condition on the fixed impermeable bottom of the lower layer is imposed as

$$W + Ud_x = 0 \quad (z = -h - d) \quad (7)$$

Based on the assumption of weak viscosity, the rotational velocities are neglected entirely near the bottom boundary.

2.2 Derivation of Boussinesq Equations

The continuity and Navier-Stokes equations for the two-layer density stratified system of flow of the incompressible fluids and the boundary conditions cited in the previous section provide a complete description of the present model. A perturbation from long wave theory to include the effects of frequency dispersion and viscosity, consistent with Boussinesq theory, is carried out to facilitate the approximate solutions to the above equations. As a first step of formulations, the following non-dimensional variables are introduced in terms of characteristic frequency ω , characteristic wave amplitude a_0 , and characteristic water depth h_0 :

$$x' = \frac{\omega x}{\sqrt{gh_0}}, y' = \frac{\omega y}{\sqrt{gh_0}}, z' = \frac{z}{h_0}, t' = \omega t, u' = \frac{h_0 u}{a_0 \sqrt{gh_0}}, U' = \frac{h_0 U}{a_0 \sqrt{gh_0}}$$

$$h' = \frac{h}{h_0}, d' = \frac{d}{h_0}, \zeta' = \frac{\zeta}{a_0}, \xi' = \frac{\xi}{a_0}, p_1' = \frac{p_1}{\rho_1 g a_0}, p_2' = \frac{p_2}{\rho_2 g a_0} \quad (8)$$

In addition, the following two length ratios are defined:

$$\varepsilon = a_0/h_0 \quad \mu = \omega^2 h_0/g \quad (9)$$

Introducing the potential ϕ for the upper layer and Φ for the lower layer, and substitution of these variables into the governing equations reduces to the following non-dimensional forms after some manipulations:

$$\mu^2 \phi_{xx} + \phi_{zz} = 0 \quad (-h + \varepsilon \xi \leq z \leq \varepsilon \zeta) \quad (10)$$

$$\mu^2 \Phi_{xx} + \Phi_{zz} = 0 \quad (-d - h \leq z \leq -h + \varepsilon \xi) \quad (11)$$

$$\varepsilon \phi_t + z + \frac{1}{2} \varepsilon \left[\phi_x^2 + \frac{1}{\mu^2} \phi_z^2 \right] = -p_1 \quad (-h + \varepsilon \xi \leq z \leq \varepsilon \zeta) \quad (12)$$

$$\varepsilon \Phi_t + z + \frac{1}{2} \varepsilon \left[\Phi_x^2 + \frac{1}{\mu^2} \Phi_z^2 \right] = -p_2 \quad (-d - h \leq z \leq -h + \varepsilon \xi) \quad (13)$$

$$p_1 = 0 \quad (z = \varepsilon \zeta) \quad (14)$$

$$\varepsilon \zeta_t + \varepsilon \mu^2 \zeta_x \phi_x - \phi_z = 0 \quad (z = \varepsilon \zeta) \quad (15)$$

$$p_1 - \frac{2}{\mu^2} \rho_1 \nu_1 \phi_{zz} = p_2 - \frac{2}{\mu^2} \rho_2 \nu_2 \Phi_{zz} \quad (z = -h + \varepsilon \xi) \quad (16)$$

$$\phi_{xz} + \Phi_{xz} = 0 \quad (z = -h + \varepsilon \xi) \quad (17)$$

$$\mu^2 d_x \Phi_x + \Phi_z = 0 \quad (z = -d - h) \quad (18)$$

For convenience the primes will be dropped from here on. The smallness parameters ε and μ are the measures of non-linearity and frequency dispersion respectively, and ε and μ^2 are assumed to be of the same order. This implies that the scales of water and mud depths are small compared to the horizontal scale, and that the free surface and interface displacements are also small compared to the depths of upper and lower layers respectively. The effect of viscosity is considered to be relatively weak in both layers and of the order of ε . The upper fluid is further assumed much less viscous than the lower mud such that the ratio of kinematic viscosity $\nu_1/\nu_2 = O(\varepsilon^2)$. This condition leads that the shear in the lower layer is entirely negligible at the interface (Hill and Foda, 1996). The vertical rotational velocity is zero to the leading order at the interface.

Integrating the continuity equations from the solid bottom to the interface, and from interface to the free surface, and applying the kinematic boundary conditions we get

$$\frac{\partial \zeta}{\partial t} + \frac{\partial}{\partial x} \int_{-h+\varepsilon \zeta}^{\varepsilon \zeta} u \, dz + \frac{\partial}{\partial x} \int_{-h-d}^{-h+\varepsilon \zeta} U \, dz = 0 \tag{19}$$

$$\frac{\partial \xi}{\partial t} + \frac{\partial}{\partial x} \int_{-h-d}^{-h+\varepsilon \zeta} U \, dz = 0 \tag{20}$$

Similarly the momentum equations can be integrated over each fluid layer to give (see Mei, 1983)

$$\frac{\partial}{\partial t} \int_{-h+\varepsilon \zeta}^{\varepsilon \zeta} u \, dz + \varepsilon \frac{\partial}{\partial x} \int_{-h+\varepsilon \zeta}^{\varepsilon \zeta} uu \, dz + \frac{\partial}{\partial x} \int_{-h+\varepsilon \zeta}^{\varepsilon \zeta} p_1 \, dz + p_1|_{-h+\varepsilon \zeta} \frac{\partial(\varepsilon \zeta)}{\partial x} = 0 \tag{21}$$

$$\frac{\partial}{\partial t} \int_z^{\varepsilon \zeta} w \, dz + \varepsilon \frac{\partial}{\partial x} \int_z^{\varepsilon \zeta} uw \, dz - \frac{\varepsilon}{\mu^2} w^2 + g(\zeta - \frac{z}{\varepsilon}) - p_1 = 0 \tag{22}$$

$$\frac{\partial}{\partial t} \int_{-h-d}^{-h+\varepsilon \zeta} U \, dz + \varepsilon \frac{\partial}{\partial x} \int_{-h-d}^{-h+\varepsilon \zeta} UU \, dz + \frac{\partial}{\partial x} \int_{-h-d}^{-h+\varepsilon \zeta} p_2 \, dz - p_2|_{-h+\varepsilon \zeta} \frac{\partial(\varepsilon \zeta)}{\partial x} - p_2|_{-h-d} \frac{\partial d}{\partial x} = 0 \tag{23}$$

$$\frac{\partial}{\partial t} \int_z^{-h+\varepsilon \zeta} W \, dz + \varepsilon \frac{\partial}{\partial x} \int_z^{-h+\varepsilon \zeta} UW \, dz - \frac{\varepsilon}{\mu^2} W^2 + g(-\frac{h}{\varepsilon} + \xi - \frac{z}{\varepsilon}) + p_2|_{-h+\varepsilon \zeta} - p_2 = 0 \tag{24}$$

The horizontal velocities u and U may be expanded as Taylor series about the interface and the solid bottom respectively. The resultant horizontal velocities can be expressed in terms of layer-averaged velocities \bar{u} and \bar{U} for both layers as

$$u = \bar{u} - \mu^2 \left[\left\{ \frac{1}{2}(z+h)^2 - \frac{1}{6}h^2 \right\} \frac{\partial^2 \bar{u}}{\partial x^2} \right] + \mu^2 \left[\left\{ (z+h) - \frac{1}{2}h \right\} \frac{\partial^2 (d\bar{U})}{\partial x^2} \right] + O(\mu^4) \tag{25}$$

$$\begin{aligned}
 U = \bar{U} - \mu^2 \left[\left\{ \frac{1}{2}(z+d+h)^2 - \frac{1}{6}d^2 \right\} \frac{\partial^2 \bar{U}}{\partial x^2} \right] - \mu^2 \left[\left\{ (z+d+h) - \frac{1}{2}d \right\} \frac{\partial d}{\partial x} \frac{\partial \bar{U}}{\partial x} \right] \\
 - \mu^2 \left[\left\{ (z+d+h) - \frac{1}{2}d \right\} \frac{\partial}{\partial x} \left(\frac{\partial d}{\partial x} \bar{U} \right) \right] + O(\mu^4) \quad (26)
 \end{aligned}$$

The horizontal velocities vary quadratically over each layer to this order. The corresponding expressions for vertical velocities are obtained from the continuity equation as

$$w = \frac{\partial \xi}{\partial t} - \mu^2 (z+h) \frac{\partial \bar{u}}{\partial x} + O(\mu^4) \quad (27)$$

$$W = -\mu^2 \left[(z+h+d) \frac{\partial \bar{U}}{\partial x} + \bar{U} \frac{\partial d}{\partial x} \right] + O(\mu^4) \quad (28)$$

Substituting Eq.(25) to Eq.(28) into the layer-integrated continuity and momentum equations (19)-(24) and retaining the terms up to $O(\epsilon)$ and $O(\mu^2)$, a set of Boussinesq-type equations can be obtained for the adopted coupled two-layer density stratified system. This set of equations is given in terms of physical variables for the three-dimensional problem as

$$\zeta_t + \nabla \cdot [(h + \zeta - \xi) \bar{\mathbf{u}}] + \nabla \cdot [(d + \xi) \bar{\mathbf{U}}] = 0 \quad (29)$$

$$\xi_t + \nabla \cdot [(d + \xi) \bar{\mathbf{U}}] = 0 \quad (30)$$

$$\bar{\mathbf{u}}_t + (\bar{\mathbf{u}} \cdot \nabla) \bar{\mathbf{u}} + g \nabla \zeta - \left[\frac{1}{3} h^2 \nabla (\nabla \cdot \bar{\mathbf{u}}_t) + \frac{1}{2} h \nabla (\nabla \cdot (d \bar{\mathbf{U}}_t)) \right] = \mathbf{0} \quad (31)$$

$$\begin{aligned}
 \bar{\mathbf{U}}_t + (\bar{\mathbf{U}} \cdot \nabla) \bar{\mathbf{U}} + (1 - \frac{1}{\gamma}) g \nabla \xi + \frac{1}{\gamma} g \nabla \zeta + \left[\frac{1}{6} d^2 \nabla (\nabla \cdot \bar{\mathbf{U}}_t) - \frac{1}{2} d \nabla (\nabla \cdot (d \bar{\mathbf{U}}_t)) \right] \\
 - \frac{1}{\gamma} \left[h \nabla (\nabla \cdot (d \bar{\mathbf{U}}_t)) + \frac{1}{2} h^2 \nabla (\nabla \cdot \bar{\mathbf{u}}_t) \right] - 2(v_2 - \frac{1}{\gamma} v_1) \nabla (\nabla \cdot \bar{\mathbf{U}}) = \mathbf{0} \quad (32)
 \end{aligned}$$

where γ is the density ratio defined as $\gamma = \rho_2 / \rho_1$, and $\bar{\mathbf{u}}$ and $\bar{\mathbf{U}}$ are the velocity vectors in upper and lower layers respectively. The model equations (29)-(32) yield the standard Boussinesq equations if all the terms involving $\bar{\mathbf{U}}$ are omitted.

3. NUMERICAL SIMULATION

Eq.(29) to Eq.(32) are solved using a finite difference scheme. The spatial derivatives in one direction are approximated using a 5-grid-points centered differences with fourth-order accuracy, leading to a truncation error that is sufficiently small relative to all the terms retained in the equations. For the temporal integral, an iterative scheme based on Adams-Bashforth-Moulton method is employed. The free surface displacement ζ and interfacial displacement ξ are

computed explicitly from the continuity equations (29) and (30). The velocity components in x -direction are computed implicitly from the momentum equations (31) and (32), treating the derivatives of \bar{u} and \bar{U} in y -direction as explicit. Similarly, the computations of velocities in y -direction are done implicitly from momentum equations, treating the derivatives of \bar{v} and \bar{V} in x -direction as explicit.

At the incident boundary, both ζ and \bar{u} are assumed to be given as input, and all the outgoing waves are absorbed applying radiation condition prescribed from the linear long wave theories. A harbour with fully reflective boundaries is treated as the solid walls and the velocity normal to the wall is taken as zero.

4. EXPERIMENTAL INVESTIGATION

Experiments were conducted to investigate the behavior of fluid mud in the harbour. The detailed experimental setup is shown in Fig.2. A laboratory wave flume of 26.0 m long, 0.60 m wide and 1.20 m high with glass walls throughout was used for the experiments. A model of rectangular harbour was installed on the horizontal bottom at 5.2 m apart from the step of the flume. A harbour basin, 50 cm long and 20 cm wide has straight breakwaters at both sides of its entrance. The experiments were also conducted for the rectangular harbour without breakwater. The harbour walls were made of acrylic fiber, so that the motions of the water surface and interface can be observed using a video camera through glass walls of the wave flume. A false bottom inside the harbour was lower than the horizontal bottom by 5cm. The hollow 5cm deep was filled with mud.

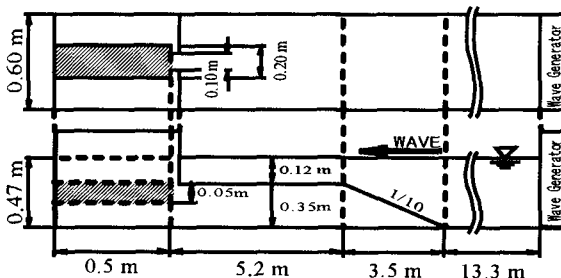


Fig.2. Experimental setup

The commercially available fine silts of mean diameter 50 μm were used to prepare the fluid mud for the experiments. Silts were mixed with water to make a well-mixed slurry of density about $\rho_2 = 1.2 \text{ g/cm}^3$. The slurry was then gently poured into the harbour to fill the requisite depth of 5.0 cm. The harbour mouth was tightly fenced from the outside before filling up water to the required depth. After filling, the mud layer in the harbour was stirred again and allowed to settle half a day. The muddy water above the interface was removed before experiments. This procedure was repeated for each experimental run to keep the requisite depth of fluid mud. By taking samples through the mud layer, only the depth-averaged density ρ_2 is measured during the experiment.

The water depth over the fluid mud bed was kept at $h = 12\text{cm}$. A monochromatic wave with the wave height $H = 1.5\text{ cm}$ was used as an incident wave for wave periods T ranging from 0.8 s to 2.0 s. Wave gauges were used to record the temporal surface wave profiles at several locations of the flume including the corner of the harbour. At the same time, the spatial profiles of the free surface and interfacial waves over the longer side of the harbour were recorded with a digital video camera through the glass walls. The interfacial displacements at the corner of the harbour were read out from the enlarged video pictures.

5. MOTION OF FLUID MUD

The observed responses of fluid mud in the harbour for various wave periods were compared with the numerical predictions for the purposes of model evaluation. In the numerical calculations the measured water surface profiles ζ were used as input data on the upwave control surface, and the corresponding horizontal velocities \bar{u} were given from the linear long wave theory. The results were, however, essentially identical to the predictions based on sinusoidal profiles ζ as input. Viscosity measurements of fluid mud were not made in the laboratory experiments. Ting and Lemasson (1996) showed from rheological tests that the viscosity of fluid mud confined within a submerged rectangular trench was not significantly affected by shear rate and time of shearing in the low strain-rate region. Since the strain rates in fluid mud under the present wave conditions were still relatively small, the viscosity ν_2 was determined from their rheological tests using the asymptotic values at low shear rate as a function of mud density.

Fig.3 shows the snapshot of the computed free-surface and interfacial displacements in the harbour without breakwater. The line $X=0$ in the figure indicates the end of the

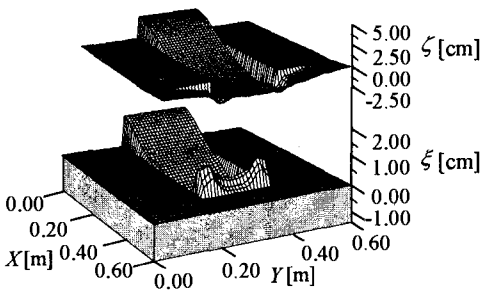
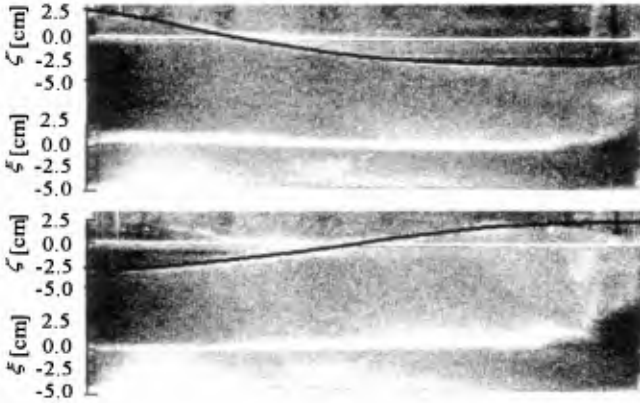


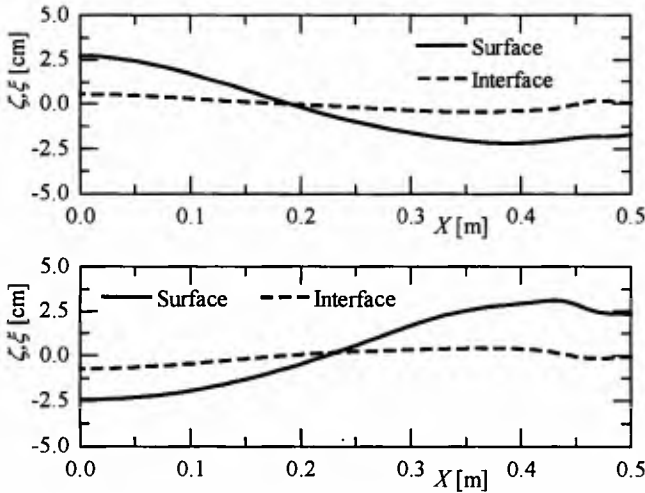
Fig.3. Snapshot of free surface and interfacial profiles
 $(T=0.8\text{s}, \rho_2=1.19\text{ g/cm}^3, \nu_2=16.4\text{ cm}^2/\text{s})$

harbour. The figure is plotted for $T=0.8\text{s}$, which corresponds to the second peak of the resonant oscillations in the harbour. The oscillations of dense mud layer appear to be almost in phase of the free-surface profiles.

Fig.4 shows the comparison of spatial profiles of the free-surface and the interfacial displacements along the longer side of the harbour. Upper and lower figures show the



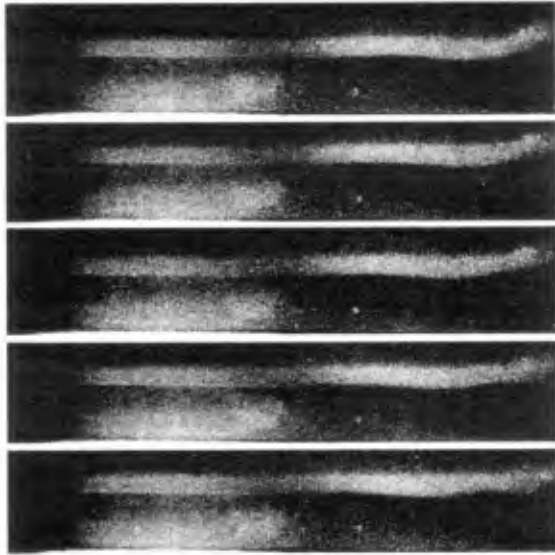
(a) Measured profiles



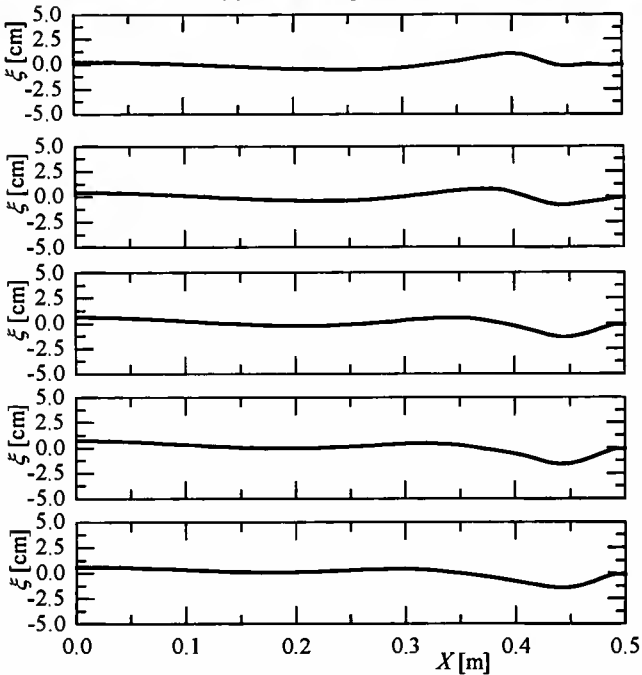
(b) Numerical profiles

Fig.4. Spatial profiles ($T=0.8s$, $\rho_2=1.19 \text{ g/cm}^3$, $\nu_2=16.4 \text{ cm}^2/s$)

images respectively when the water surface displacements become maximum at the corner of the harbour and $T/2$ after that time. The surface mode of the interfacial waves governs the motion of the interface and the interface oscillates nearly in phase of surface waves. At the entrance of the harbour, small internal waves out of phase are observed both in the experimental and numerical results, but they quickly absorb their energy within a very short distance from the harbour mouth.



(a) Measured profiles



(b) Numerical profiles

Fig. 5. Spatial profiles ($T=1.2\text{s}$, $\rho_2=1.19\text{ g/cm}^3$, $\nu_2=16.4\text{ cm}^2/\text{s}$)

The sequence of pictures at intervals of 0.1s for the wave period of 1.2s is shown to demonstrate the motion of fluid mud inside the harbour in Fig.5. It is observed from both experimental and numerical profiles that the interfacial waves are first generated at the harbour mouth, and propagate at internal phase speed towards the harbour end. The amplitudes of the interfacial waves are substantially reduced in course of their propagation due to the energy dissipation. The phase of the numerically simulated profiles is slightly delayed from the experimental profiles.

Fig.6 shows the comparison of spatial profiles for $T=1.6s$ which corresponds nearly to the first peak of resonant oscillations in the harbour without breakwater. Distinct

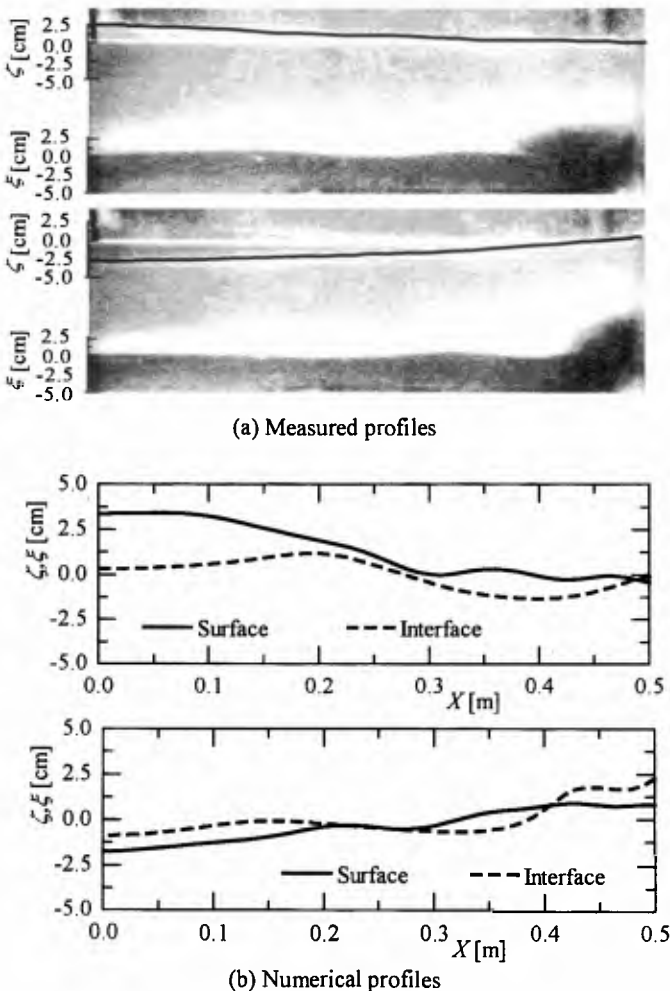


Fig.6. Spatial profiles ($T=1.6s, \rho_2=1.19 \text{ g/cm}^3, \nu_2=16.4 \text{ cm}^2/\text{s}$)

internal waves at the interface are observed in this case and the internal mode of the interfacial waves dominates the motion of the interface. Both the experimental and numerical results indicate that the internal wave generated at the harbour mouth propagates towards the harbour end without much dissipation. The amplification of the free-surface displacements inside the harbour is significantly reduced in this case. As shown in Fig.6 (a), the mud bed is strongly stirred up due to the vortex formed at the harbour mouth. The response of fluid mud to wave action may no longer be described by the two-layer model due to this suspended sediment. The present model must be modified for quantitative accuracy.

6. AMPLIFICATION FACTOR

The experimental and numerical results for the amplification factor of the water surface and interfacial displacements are shown in Fig.7 for the harbour without breakwater. The amplification factor is defined as the ratio of wave height H at the corner of the harbour to the incident surface wave height H_i and plotted as a function of the ratio of the harbour length l to the length of incident wave L , with L being determined from linear wave theory. The results for the harbour with breakwaters at

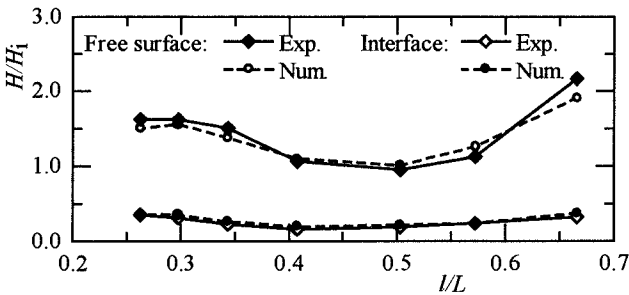


Fig.7. Amplification factors at the corner of harbour without breakwater

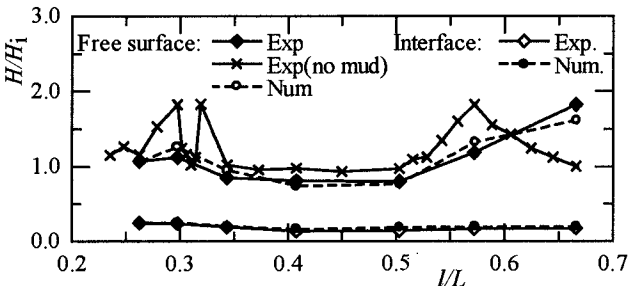


Fig.8. Amplification factors at the corner of harbour with breakwater

the entrance are shown in Fig.8. Two peaks observed near the first mode of the resonant oscillations without fluid mud bed is due to the effects of side walls of the wave flume. The amplifications of the water surface waves are significantly reduced

near the first peak of the resonant oscillations where the interfacial displacements governed by the internal mode increase to the maximum. At the secondary peak, the surface mode governs the motion of the interfacial waves, and thus the interface oscillates nearly in phase of the surface wave. In this case, the secondary peak for the water surface displacements shifts to the higher frequency with the apparent increase in water depth by the thickness of mud layer. The amplification factors decrease to a limited extent at the secondary peak.

7. CONCLUDING REMARKS

Behaviors of fluid mud in a harbour basin for various wave periods are investigated both experimentally and numerically. The study reveals that the amplification of water surface waves is significantly reduced near the fundamental peak of long-period oscillations, where the internal mode governs the motion of fluid mud. In the frequency range higher than secondary peak, the surface mode governs the motion of the interface, yielding an insignificant reduction in the amplification factor.

REFERENCES

- Dalrymple, R. A., and Liu, P. L. -F (1978). "Waves over soft muds: A two-layer fluid model", *J. Phys. Oceanogr.*, Vol.8, pp.1121-1131.
- Foda, M. A., Hunt, J. R., and Chen, H. T. (1993). "A nonlinear model for the fluidization of marine mud by waves", *J. Geophys. Research.*, Vol.98, pp.7039-7047.
- Hill, D. F., and Foda, M. A. (1996). "Subharmonic resonance of short internal standing waves by progressive surface waves", *J. Fluid Mech.*, Vol.321, pp.217-233.
- Mei, C. C. (1983). "The applied dynamics of ocean surface waves", *John Wiley, New York*, 740p.
- Takahashi, S., Shimosako, K., Yamamoto and Miura, H. (1994). "Small-scale experiments on a boiling sand bed and its wave absorbing effects", *Proc. of Coastal Eng., JSCE*, Vol.41, pp.611-615 (in Japanese).
- Ting, F. C. K., and Lemasson, W. J. (1996). "Dynamic response of fluid mud in a submarine trench to water waves", *Coastal Engineering*, Vol.27, pp.97-121.